Journal of ELECTRONIC MATERIALS, Vol. 49, No. 12, 2020
https://doi.org/10.1007/s11664-020-08460-9

Enhanced Microwave Absorption Performance of SWCNT/SiC Composites

SAMARJIT SINGH,[1] ABHISHEK KUMAR ,[1,3] and DHARMENDRA SINGH[2]

1.—Department of Applied Mechanics, Motilal Nehru National Institute of Technology Allahabad, Prayagraj, India. 2.—Department of Electronics and Computer Engineering, Indian Institute of Technology Roorkee, Roorkee, India. 3.—e-mail: abhishek@mnnit.ac.in

The present work emphasizes the microwave absorption performance of single-walled carbon nanotube (SWCNT)/SiC composites prepared by mechanically mixing the components, i.e., SWCNT and SiC in desired weight fractions using a cost-effective and simple ball-milling route. The microwave absorption results reveal that the integration of SiC with a small weight fraction of SWCNT exhibited an improved absorption performance in the K_u band compared to pristine SiC. The SWCNT/SiC composite with 2.5 wt.% SWCNT exhibited a superior microwave absorption behavior with a minimum reflection loss of − 37.11 dB and < − 10 dB absorption bandwidth of 4.38 GHz for the absorber thickness of 2 mm. The microwave absorption efficiency of SWCNT/SiC composites was also measured corresponding to − 10 dB, which is equivalent to 90% microwave absorption when evaluating the absorption performance. A maximum microwave absorption efficiency of 18.95 dB GHz/mm was observed for the composite with 2.5 wt.% SWCNT dispersion compared to 3.4 dB GHz/mm for pristine SiC. Enhanced microwave absorption characteristics for SWCNT/SiC composites may be attributed to various absorption mechanisms, such as dipole polarization, multiple scatterings, multiple reflections, conductive loss, interfacial polarization, and defect-induced dipole polarization. The microwave absorption results of SWCNT/SiC composites indicate that they may serve as encouraging thin thickness candidates with superior microwave absorption for application in the K_u band.

(Received June 25, 2020; accepted August 28, 2020; published online September 14, 2020)

Graphic Abstract

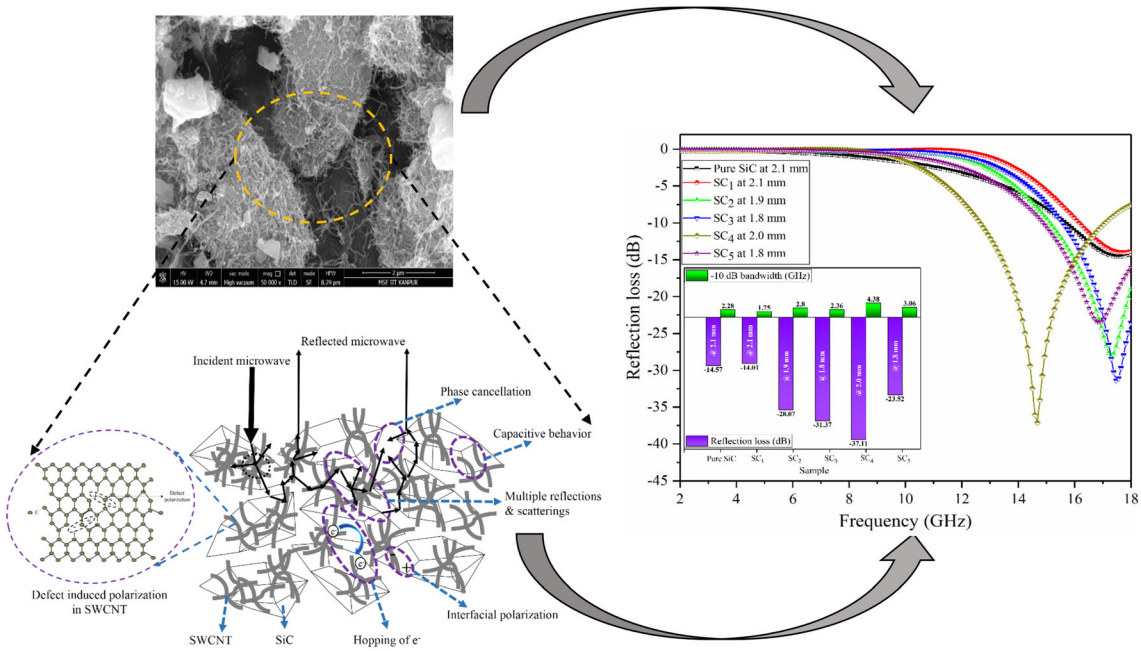

Key words: SiC, SWCNT, microwave absorption, reflection loss, interfacial polarization, multiple reflections

INTRODUCTION

Electronic equipment has become the backbone of modern society, covering every walk of life, encompassing civil, military, and healthcare systems.[1,2] This upsurge in the usage of electronic gadgets has led to significant growth in the electronics sector. However, the extensive use of electronic systems has led to electromagnetic pollution problems.[3,4] The interference of the microwave signals of various electronic systems affects the operational functionality of telecommunication and electronic appliances. The electromagnetic pollution problem not only interferes with the proper functioning of electronic appliances but it also poses serious health issues by causing various life-threatening diseases.[5] The severity of the situation has given rise to the need to develop high-performance microwave absorbing materials to tackle the electromagnetic interference problems. Apart from minimizing the interference problems, microwave absorbing and shielding materials have also attracted the attention of researchers in other areas of application which include imparting stealth features to military vehicles, aircraft, drones, and various warheads by reducing the radar cross-section, radome structures, cloaking, and satellite communications.[6–9] The progress in materials science and technology has witnessed significant improvements in the development of microwave absorbing materials and structures with different morphological and geometrical designs. Significant progress has been made in the development of nanocomposites and frequency selective surfaces-based microwave absorbing materials and structures with broadband frequency response.[10–13]

The importance of microwave absorbing materials in civil, satellite communications and defense-related fields has propelled scientific minds to develop innovative ideas for the production of efficient absorbers with strong microwave absorption, thin thickness, and broadband frequency response. However, a single conventional material alone cannot demonstrate all these favorable traits. This has encouraged significant research towards the development of composite materials for realizing enhanced microwave absorption. In the past, there has been significant research on the development of ferrite- and magnetic metal-based materials, i.e., Ni-Zn ferrites,[14] $BaFe_{12}O_{19}$,[15] Ni,[16] Fe,[16] Fe_3O_4,[16] etc. However, these magnetic materials have certain limitations, such as high density and loss of ferromagnetic characteristics beyond the Curie temperature.[16,17] These limitations have engaged the attention of researchers toward ceramic- and carbon-based materials, such as SiC, ZnO, CNT,

graphene, graphene oxide, etc., which do not suffer the limitations of magnetic-based microwave absorbers. Among the ceramic candidates, SiC is an excellent dielectric material having the ability to perform satisfactorily in harsh environments.[5,18] However, pure SiC does not exhibit a good microwave absorption performance because of its poor electrical conductivity.[19] Therefore, SiC needs to be combined with conductive particles to enhance its microwave absorption characteristics. This may be achieved by adding metal particles,[20] CNT, graphene, graphene oxide, etc. into the SiC system. However, the addition of metallic particles increases the density of the composites which then suffer from susceptibility to corrosion; thus, the addition of carbon-based materials may prove to be advantageous in imparting conductivity to SiC-based composites without increasing their density.

In this article, an idea has been explored to integrate SiC with varying amounts of single-walled carbon nanotubes (SWCNT) in order to enhance the dielectric and conductive losses to realize enhanced microwave absorption behavior by varying the loading concentration of SWCNT to find the optimal fraction of SWCNT needed in the SiC. Many articles have discussed the microwave attenuation behavior of multi-walled carbon nanotube (MWCNT)/SiC-based composite systems; however, to the best of the authors' knowledge, limited articles exist that discuss the absorption performance of SWCNT/SiC-based composite systems. The idea is to use the excellent electrical conductivity of SWCNT to enhance the conductive loss, dipole polarization, multiple scatterings, multiple reflections, and the interfacial polarization loss of the SWCNT/SiC composites. The various microwave attenuation mechanisms influencing the reflection loss results are discussed in detail.

EXPERIMENTATION METHODOLOGY

Materials

Analytical grade SiC powder (Moisannite 6H, 200-450 mesh) was acquired from Sigma Aldrich. The SWCNT were used in the as-received condition without subjecting them to any surface modification process.

Synthesis of SWCNT/SiC Composites

The as-received SWCNT were ultrasonicated for 1 h with acetone to minimize the agglomeration tendency. Varying weight fractions of the ultrasonicated SWCNT, i.e., 0.5 wt.%, 1 wt.%, 2 wt.%, 2.5 wt.%, and 3 wt.%, were then dispersed in the SiC to synthesize SWCNT/SiC composites. A planetary ball mill (PM 100; Retsch) was employed to mix the two components using an agate jar and balls at 100 rpm for 1 h. A ball to powder ratio of 10:1 was used for the mixing operation in the acetone medium. The synthesized composites were further manually homogenized with the help of a mortar and pestle for 30 min. The synthesized SWCNT/SiC composites with varying SWCNT content were finally vacuum-dried at 60°C for 24 h. The prepared composites were coded as SC_1, SC_2, SC_3, SC_4, and SC_5 for the 0.5 wt.%, 1 wt.%, 2 wt.%, 2.5 wt.%, and 3 wt.% SWCNT dispersions, respectively.

Instruments and Measurements

Phase identification of the synthesized SWCNT/SiC composites was ascertained by employing the x-ray diffraction (XRD) technique using an X-ray diffractometer (Rigaku Smartlab) in the 10°–90° scanning range. Raman spectra of the composites were recorded using a WI-Tec Raman spectrometer (XMB3000-3000) with an excitation wavelength of 633 nm of an Argon ion laser in the 600–3000 cm^{-1} spectral range. Morphological structures and features of the composites were investigated by analyzing the micrographs obtained from a Quanta 200 field-emission scanning electron microscopy (FE-SEM). Transmission electron microscopy (TEM) of the SWCNT was performed to ascertain the single-walled characteristics of the purchased product. An image processing tool, ImageJ, was used to examine the FE-SEM and TEM micrographs to measure the morphological dimensions. Investigation of microwave absorption characteristics of SWCNT/SiC composites was conducted with the help of dielectric measurement. The typical coaxial method was employed for the measurement of the dielectric parameters, i.e., complex permittivity and permeability using vector network analyzer (VNA; Agilent N5222 PNA series) in the 2–18 GHz range. The dielectric measurement for all the composite samples was carried out by casting cylindrical pellets. The powder composite samples were mixed with epoxy resin by weight fractions in an 80:20 ratio. Cylindrical pellets of 7 mm outer diameter and 3.04 mm inner diameter were cast from the powder-epoxy mixtures. Before carrying out the actual measurements, the calibration of the VNA setup was carried out by following the standard calibration procedure for coaxial measurements to null out the systematic errors arising from cables, connectors, etc., and air gap corrections were made so that the VNA could provide the highest possible accuracy for its test results.

RESULTS AND DISCUSSION

Phase analysis

The XRD technique was used to analyze and characterize the phase and composition of the synthesized SWCNT/SiC composites. The diffraction patterns of the composites demonstrate the existence of diffraction peaks corresponding to SiC and carbon (C), as shown in Fig. 1. The phase analysis identified the hexagonal crystal structure of SiC (ICSD: 27051). With the addition of SWCNT

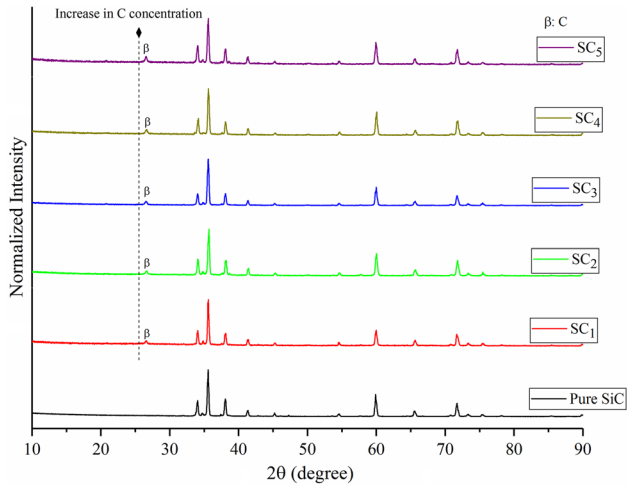

Fig. 1. Phase identification of pure SiC and synthesized SWCNT/SiC composite samples with varying SWCNT concentration using x-ray diffraction patterns.

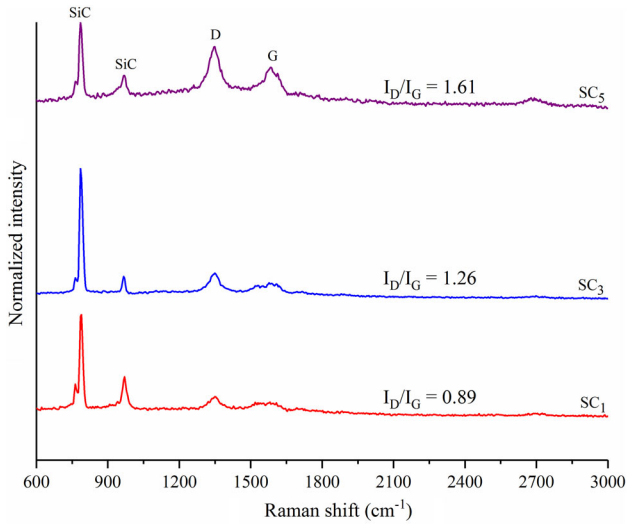

Fig. 2. Raman spectra of selected SWCNT/SiC composite samples.

in SiC, a diffraction peak corresponding to C (ICSD: 76,767) can be observed at approximately 2θ 26.5°, which indicates the presence of SWCNT in the composites. It can also be observed from Fig. 1 that the intensity of the diffraction peaks corresponding to C rises with the quantity of SWCNT in the composite system. The XRD patterns indicate the occurrence of characteristic peaks corresponding to SiC and C only, and no other impurity phase can be observed.

The phase confirmation was further investigated for selected SWCNT/SiC composites (i.e., SC_1, SC_3, and SC_5) using the Raman scattering spectra, as depicted in Fig. 2. The distinctive peaks at 785 cm^{-1} and 966 cm^{-1} match the 6H-SiC crystal structure which is consistent with the XRD results.[21] The presence of CNT is established by the presence of the characteristic D and G bands of CNT at the peak positions of 1347 cm^{-1} and 1586 cm^{-1}, respectively.[22] The D band is associated with the concentration of defects in the CNT, and the G band represents the degree of graphitization. The Raman spectra also assist in qualitatively evaluating the structural defects present in the dispersed SWCNT with the help of the I_D/I_G ratio.[21] The integrated intensity corresponding to the D and G bands has been calculated to measure the I_D/I_G ratio. It may be observed from Fig. 2 that the I_D/I_G ratio has increased with the increase in SWCNT concentration. The increase in the I_D/I_G ratio infers that composites with higher concentrations of SWCNT have a relatively larger number of structural defects compared to lower concentrations of SWCNT dispersed composites.

Morphological Analysis

The morphology of pure SiC and SWCNT are shown in Fig. 3. Figure 3a shows the FE-SEM micrographs of SiC particles and the average particle size was calculated to be 52 μm with non-uniform geometrical features. The SWCNT displays uniform tube-like morphological features with a large length to diameter ratio, as shown in Fig. 3b. The TEM micrograph of SWCNT shows the hollow tubular structure, as depicted in Fig. 3c. The average size of the outer and inner diameters, as measured from the TEM image, were found to be 18.8 nm and 6.3 nm, respectively. The TEM micrograph confirms the single-walled structure of the CNT.

The morphological examinations using FE-SEM of selected composites, i.e., SC_1, SC_3, and SC_5, are depicted in Fig. 4a–c, respectively. The presence of SWCNT on the surface of the SiC particles can be clearly observed in the composites. It can also be deduced from Fig. 4 that, with the rise in SWCNT concentration, larger amounts of CNT envelope the surface of the SiC particles in the composites.

Dielectric Study

The microwave absorption phenomenon is well understood with the help of microwave dielectric parameters, i.e., complex permittivity (ε_r) and permeability (μ_r). The study of microwave dielectric parameters gives an understanding of the microwave absorption mechanisms. The real part (ε' and μ') is basically used to evaluate the storage capacity of electromagnetic energy (electric and magnetic energy), while the imaginary part (ε'' and μ'') is used to evaluate the dissipation capability of electromagnetic energy. The variation of ε' for SWCNT/SiC composites in the 2–18 GHz range is depicted in Fig. 5a. Composite samples SC_4 and SC_5 show higher values of ε' compared to the pristine SiC. This increase may be ascribed to the capacitive effect due to the addition of SWCNT in the composites. The higher concentration of SWCNT in composites SC_4 and SC_5 leads to an increase in the

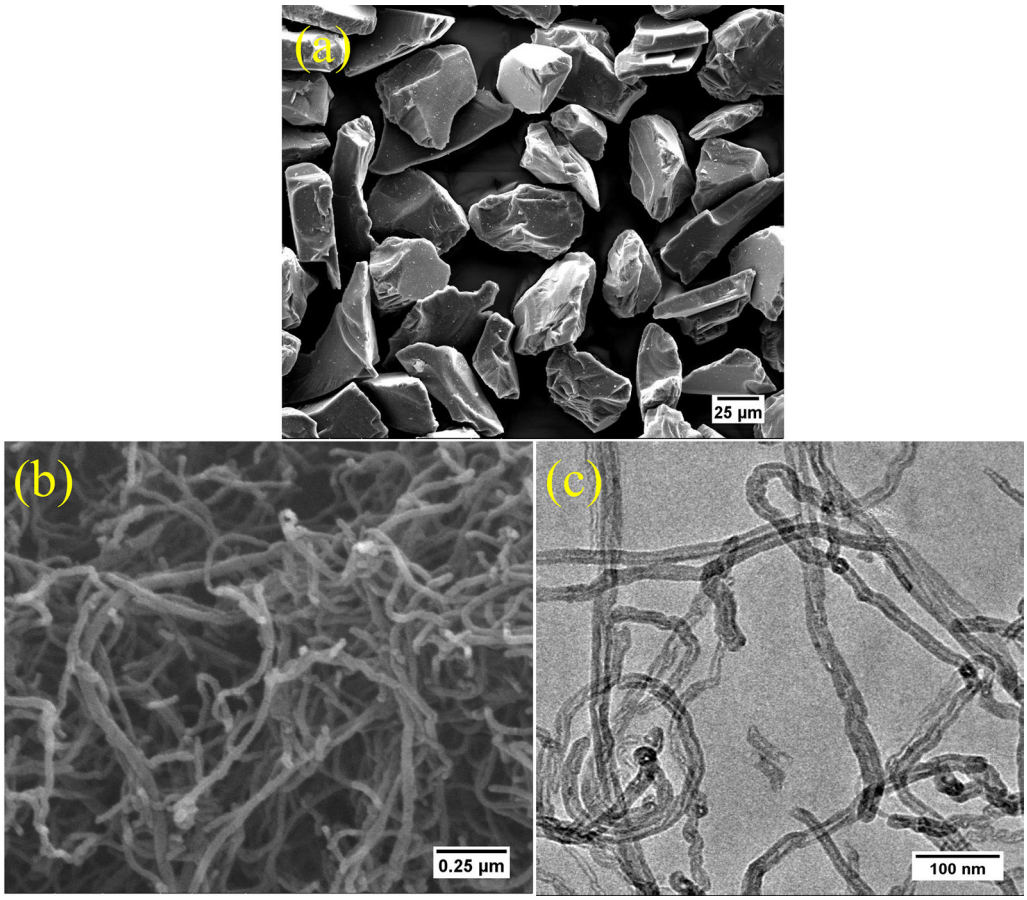

Fig. 3. Morphological representation of (a) FE-SEM micrograph of the SiC particles, (b) FE-SEM micrograph of pure SWCNT, and (c) TEM micrograph of pure SWCNT.

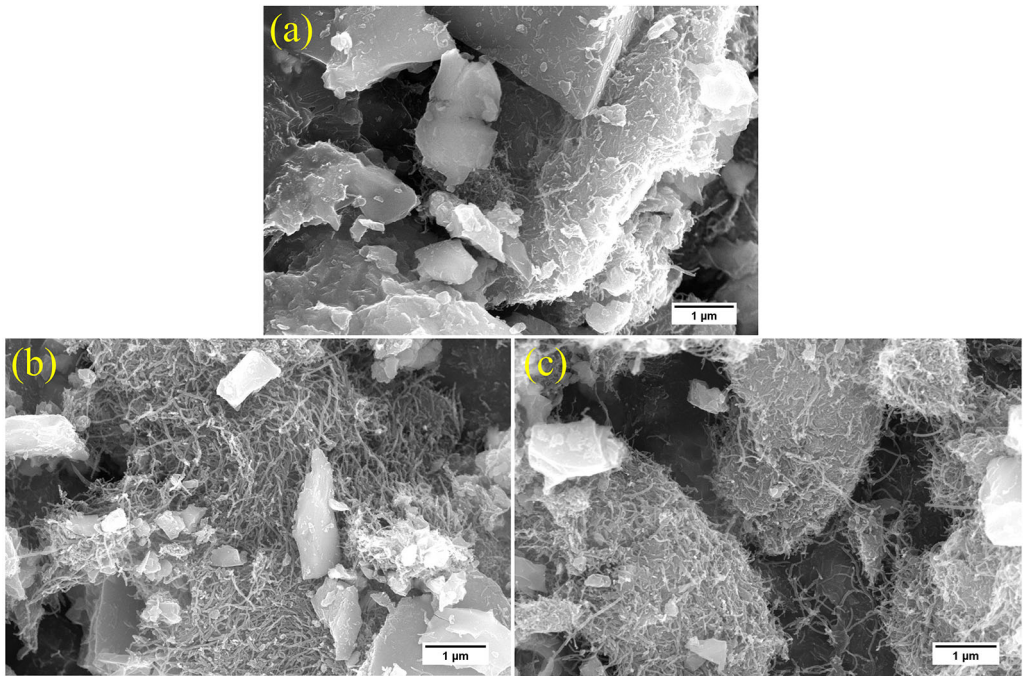

Fig. 4. Morphological analysis of selected SWCNT/SiC composite samples: (a) sample SC_1, (b) sample SC_3, and (c) sample SC_5 using FE-SEM micrographs.

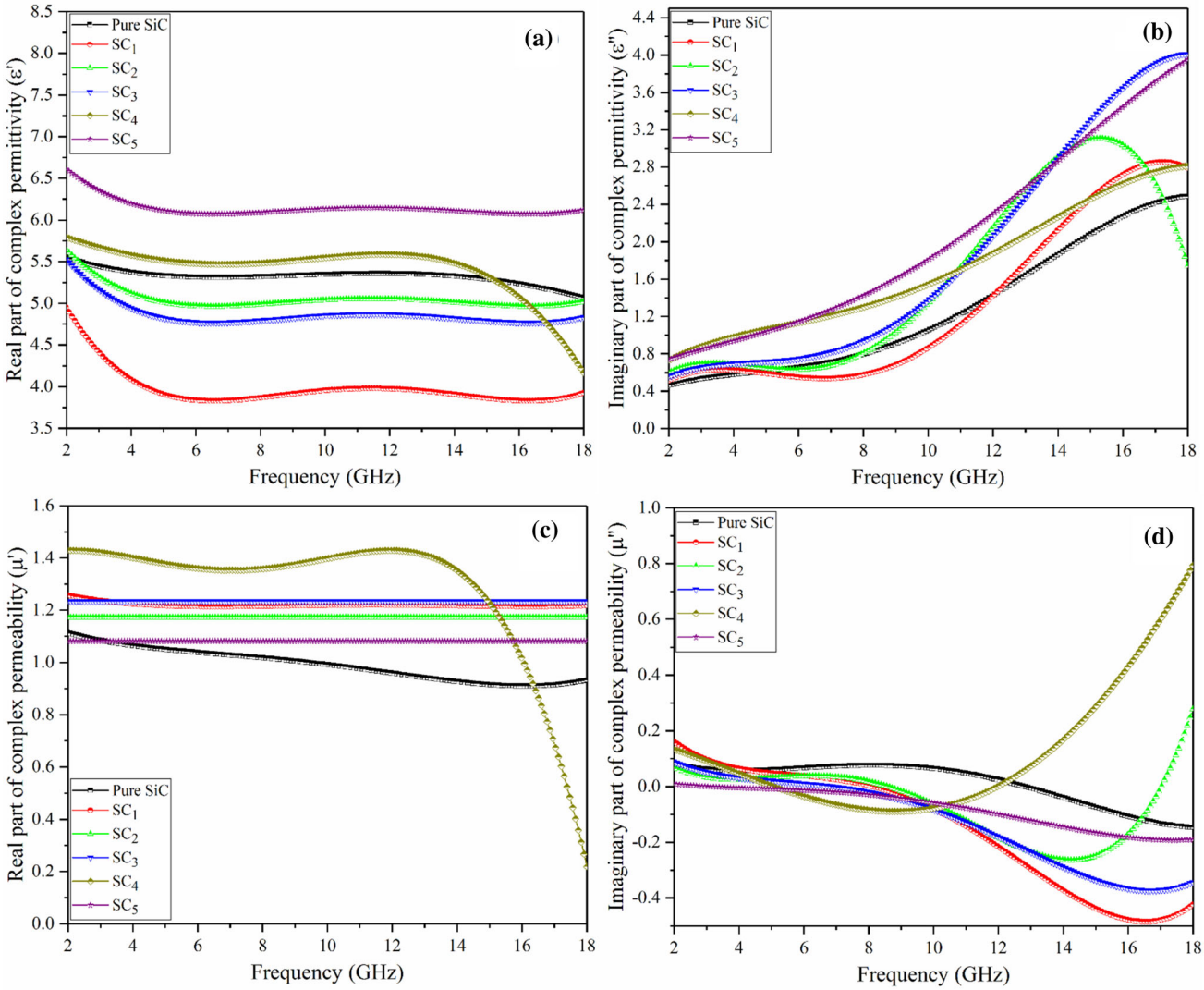

Fig. 5. Microwave dielectric frequency response of SWCNT/SiC composites in the 2–18 GHz range: (a) real part of complex permittivity, (b) imaginary part of complex permittivity, (c) real part of complex permeability, and (d) imaginary part of complex permeability.

number of micro- and nano-capacitive circuits, which trap the charge carriers resulting in the increase of ε'. The variation of ε'' for SWCNT/SiC composites in the 2–18 GHz range is depicted in Fig. 5b, from which it can be seen that the values of ε'' increase with the rise in the quantity of SWCNT in the SWCNT/SiC composite system. Higher values of ε'' indicate higher conductivity according to the free-electron theory, as represented by Eq. 1[20,23]:

$$\varepsilon'' = 1/(2\pi\varepsilon_o\rho f) \quad (1)$$

where, ρ and ε_o represent the electrical resistivity and permittivity of free space, respectively.

According to the free-electron theory, the electrical resistivity of the composites might decrease with the rise in the concentration of SWCNT. The existence of heterogeneous interfaces formed due to the presence of SiC and SWCNT in the composites with different electronegativity assist in the amassing of charge carriers at the interfaces, and the accumulation of these charges in the alternating electromagnetic field promotes interfacial polarization.[24,25] Apart from this, the presence of structural defects in SWCNT and SiC contribute to defect-induced dipole polarization. These polarizations in the composites translate into higher values of ε'' as compared to the pristine SiC system. Figure 5c represents the variation in the nature of μ' for the SWCNT/SiC composites in the 2–18 GHz range. The complex behavioral trend of μ'' with the increase in frequency can be observed from Fig. 5d, reflecting a negative trend in the values of μ'' at higher frequencies of the composites. The occurrence of negative μ'' has been observed in many composites, such as mesoporous carbon–silica nano-composites, SiC nanowires, MWCNT composites, etc.[26] The conversion of magnetic energy to electric energy in an alternating electromagnetic field is the main reason for this negative trend,[27] which, in the values of μ'', is characterized by a loss of electrical

energy according to the energy conservation principle.[27] The higher numerical values of ε'' for the SWCNT/SiC composites at higher frequencies where the negative trend in μ'' is observed maintains the consistency of the energy conservation principle.

Microwave Absorption Performance

The parameter for evaluating the microwave absorption capability of SWCNT/SiC composites is the reflection loss (RL), which is determined with the help of transmission line theory as mathematically expressed in Eqs. 2 and 3.[28,29]

$$RL\,(\mathrm{dB}) = 20\log\left|\left(Z_{\mathrm{in}} - Z_{\mathrm{o}}\right)/\left(Z_{\mathrm{in}} + Z_{\mathrm{o}}\right)\right| \quad (2)$$

$$Z_{\mathrm{in}} = Z_{\mathrm{o}}(\mu_{\mathrm{r}}/\varepsilon_{\mathrm{r}})^{frac12;}\tanh\left\{j\cdot(2\pi ft/c)\,(\mu_{\mathrm{r}}\cdot\varepsilon_{\mathrm{r}})^{frac12;}\right\} \quad (3)$$

where f represents the frequency, t is the absorber thickness, c represents the velocity of light, Z_{in} and Z_{o} represent the characteristic impedance of the composites and the free space, respectively.

The RL behavior of SWCNT/SiC composites corresponding to maximum microwave absorption at their matching thickness is shown in Fig. 6. The microwave absorption behavior of pure SiC exhibits a minimum RL value of − 14.5 dB at 17.5 GHz for an absorber thickness of 2.1 mm, as can be observed in Fig. 6. The corresponding absorption bandwidth (< − 10 dB) of 2.28 GHz absorption bandwidth is achieved for the pristine SiC system, and it can be observed from Fig. 6 that, with the increase in SWCNT concentration, the microwave absorption characteristics of SWCNT/SiC composites has significantly improved. For the developed SWCNT/SiC composites, the minimum RL value of − 37.11 dB has been realized for sample SC_4 at 14.23 GHz at 2 mm absorber thickness. The corresponding − 10 dB absorption bandwidth of 4.38 GHz is achieved for the sample. The summary of the microwave absorption properties of the SWCNT/SiC composites is shown in the inset of Fig. 6. The

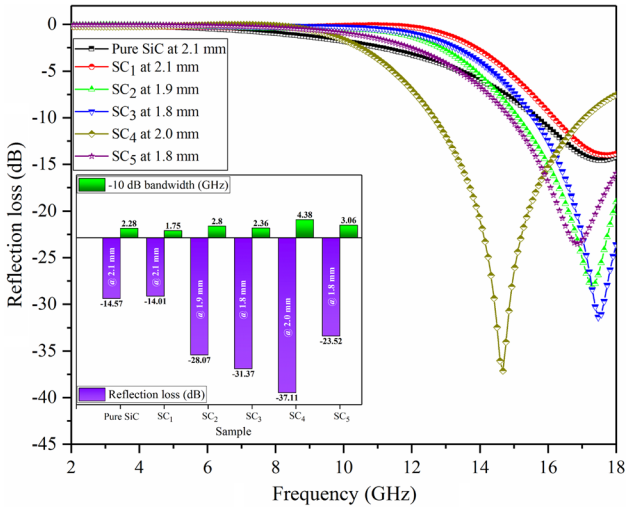

Fig. 6. Reflection loss behavior of SWCNT/SiC composites at their respective matching thicknesses with varying SWCNT concentrations. *Inset* the numerical values of the microwave absorption properties.

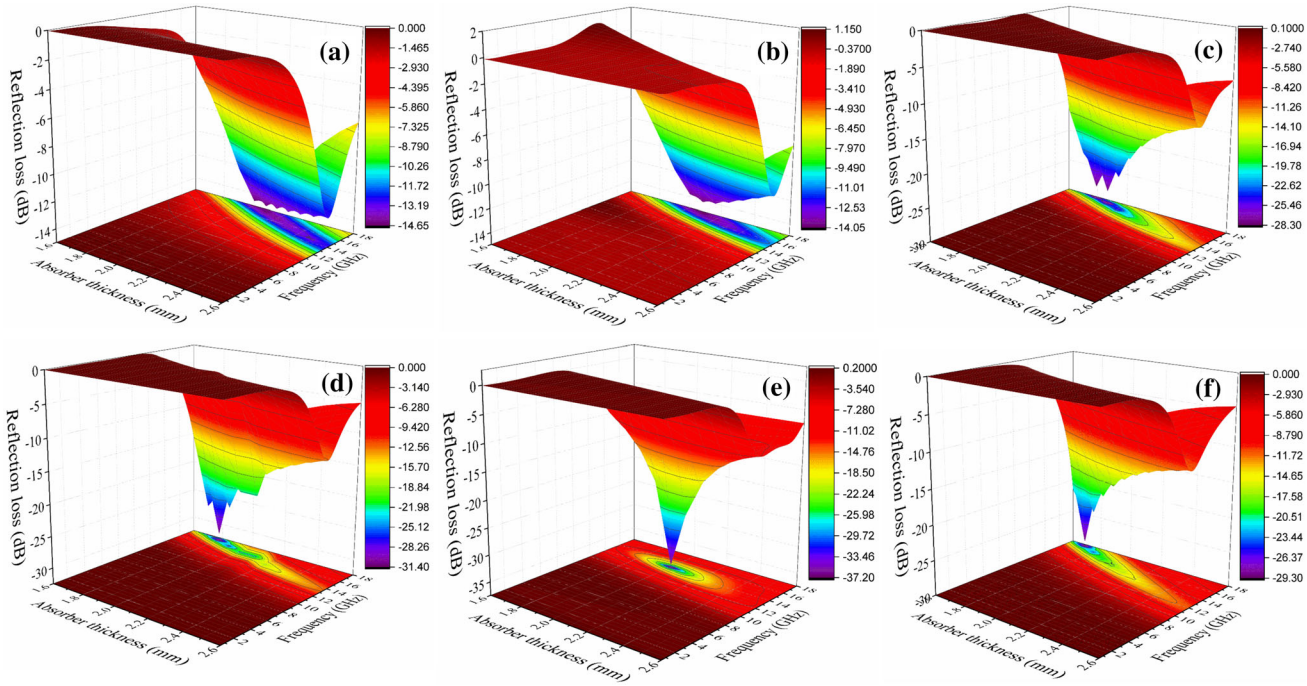

Fig. 7. 3D RL plots of SWCNT/SiC composite samples: (a) pure SiC, (b) sample SC_1, (c) sample SC_2, (d) sample SC_3, (e) sample SC_4, and (f) sample SC_5.

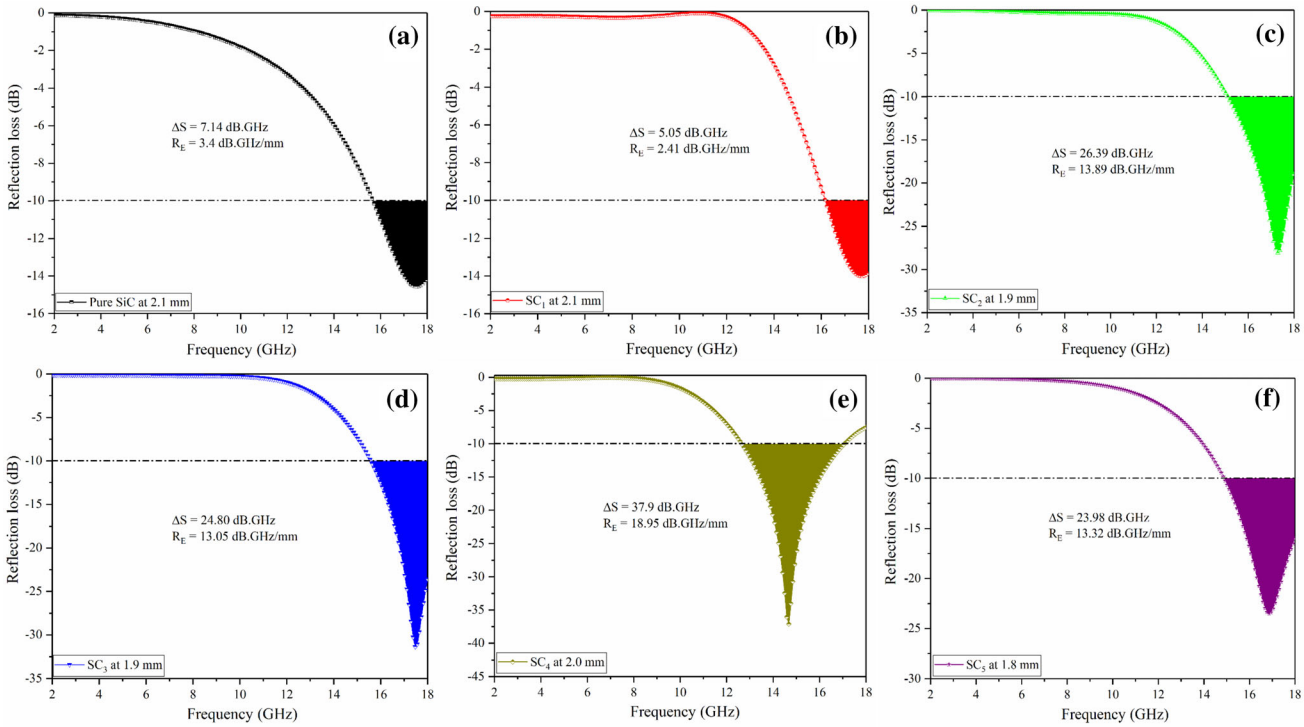

Fig. 8. Variation of the microwave absorption efficiency of SWCNT/SiC composites (a) pure SiC, (b) sample SC_1, (c) sample SC_2, (d) sample SC_3, (e) sample SC_4, and (f) sample SC_5 at their respective matching thickness.

3D surface plots of RL values with variable thickness (ranging from 1.6 mm to 2.6 mm) for SWCNT/SiC composites are shown in Fig. 7a–f. An effective microwave absorber should represent a broad < -10 dB absorption bandwidth with minimum absorber thickness. Thus, from the 3D representations of the RL results, it can be seen that samples SC_4 and SC_5 represent better microwave absorbers since they exhibit a better -10 dB absorption bandwidth for thin absorber thickness (≤ 2 mm) as compared to pure SiC and other SWCNT/SiC composites. The microwave absorption results indicate that the incorporation of SWCNT enhances the microwave absorption behavior of SWCNT/SiC composites. A good absorber should be integrated with excellent characteristics, such as high absorption, broadband frequency response, and thin thickness, and the microwave absorption efficiency (R_E) may prove to be useful in investigating the absorption performance. The usefulness of microwave absorption efficiency (R_E) may be appreciated in situations where different composites exhibit nearly similar microwave absorption characteristics, and choosing between the alternatives becomes difficult. The microwave absorption efficiency is mathematically expressed using Eq. 4[30,31]:

$$R_E = \frac{\Delta S}{d}$$
$$\Delta S = \int RL df|_{RL \leq -10dB} \quad (4)$$

where ΔS is the area corresponding to -10 dB reflection loss, and d is the absorber thickness.

Figure 8a–f represents the microwave absorption efficiency curves for the composites at their matching thicknesses. The maximum absorption efficiency value of 18.95 dB GHz/mm has been obtained for composite SC_4. It may also be observed from Fig. 6 that samples SC_2, SC_3, and SC_5 exhibit different microwave absorption characteristics, with SC_3 having a better RL value, but lower absorption bandwidth as compared to SC_2 and SC_5. Although these samples exhibit different microwave absorption properties, the R_E values of these samples are relatively close, indicating the closeness in the choice of SC_2, SC_3, and SC_5 as microwave absorbers. From the R_E values, it can be deduced that sample SC_2 would prove to be a better and more economical choice between samples SC_2, SC_3, and SC_5 because of the lower concentration of SWCNT in SC_2. Thus, it can be observed that microwave absorption efficiency can prove to be an effective parameter in the choice of efficient and economical microwave absorbers.

The dielectric loss tangent parameter is used to evaluate the loss ability of microwaves, particularly in dielectric materials. This parameter may be used to explain the enhancement in the microwave absorption characteristics of SWCNT/SiC composites, and Fig. 9 represents their dielectric loss tangents. The incorporation of SWCNT results in enhancement in the loss tangent behavior for

SWCNT/SiC composites as compared to the pristine counterpart, which translates into a better microwave absorption performance. Impedance matching and the attenuation constant constitute the other key factors for realizing strong microwave absorption behavior. The normalized impedance ($|Z_{in}/Z_o|$) decides the degree to which the incident microwaves can enter into the absorber's surface, and is mathematically represented by Eq. 5.

$$|Z_{in}/Z_o| = (\mu_r/\varepsilon_r)^{\frac{1}{2}}\tanh\{j\cdot(2\pi ft/c)(\mu_r\cdot\varepsilon_r)^{\frac{1}{2}} \quad (5)$$

The numerical value of $|Z_{in}/Z_o|$ should be close to 1 to realize better microwave absorption performance.[29] The attenuation constant (α) is another factor which represents the intrinsic ability of the absorbing material to mitigate the incident microwaves, thus, governing the microwave absorption performance; it is expressed by Eq. 6[32]:

$$\alpha = \frac{\sqrt{2}\pi f}{c}\sqrt{(\mu''\varepsilon'' - \mu'\varepsilon') + \sqrt{(\mu''\varepsilon'' - \mu'\varepsilon')^2 + (\mu'\varepsilon'' - \mu''\varepsilon')^2}} \quad (6)$$

where each symbol represents their usual meaning.

Figure 10a and b represents the normalized impedance matching and attenuation behavior of the SWCNT/SiC composites. Figure 10a reflects poor impedance matching behavior of the composites, indicating that other factors have been dominant in achieving enhanced absorption for the prepared composites. Figure 10b shows that, with the increase in SWCNT loading fraction, the attenuation behavior has significantly improved. Among the composites, SC_4 has the highest attenuation constant, resulting in maximum microwave absorption characteristics. Higher attenuation constants for the SiC composites translate into better microwave absorption compared to the pristine SiC counterpart.

The microwave absorption in SWCNT/SiC composites may be attributed to just the dielectric loss because of the presence of a dielectric/dielectric system in the composites. As no magnetic component is present in the composite system, it is expected that the role of magnetic loss mechanisms in microwave absorption is negligible. In the gigahertz frequency range, dielectric loss mainly arises due to dipole polarization, conduction loss, and interfacial polarization loss. The polarization of the materials due to dielectric polarization cannot

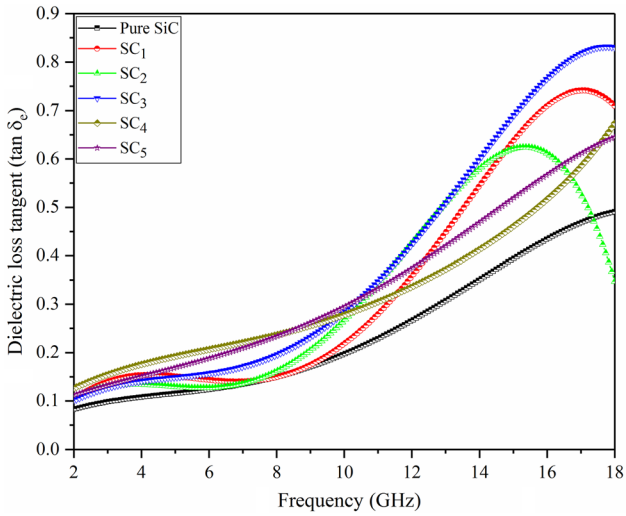

Fig. 9. Variation of dielectric loss tangent of SWCNT/SiC composite samples in the 2–18 GHz range.

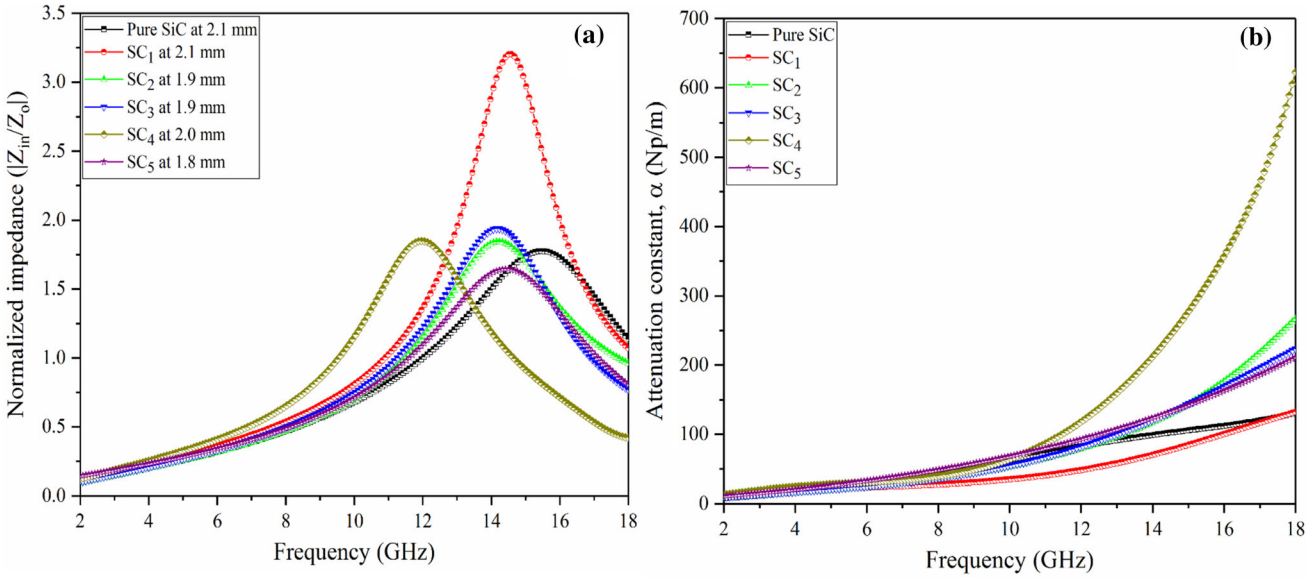

Fig. 10. Variation of (a) normalized impedance matching at matching thicknesses and (b) attenuation constants of SWCNT/SiC composite samples in the 2–18 GHz range.

be maintained in the gigahertz range with the increase in frequency.[1] This is because, at higher frequencies, the dipole moments get less time to align with the alternating microwave field; hence, some hysteresis phenomena occur during the polarization process, causing polarization relaxation loss. In order to quantify and analyze the polarization relaxation process and the dominance of dielectric properties in any Debye system, Cole–Cole curves have proven to be potent tools. The Cole–Cole curve is generated by plotting ε' and ε'' and is mathematically formulated as[1]:

$$\varepsilon' - \left(\frac{\varepsilon_s + \varepsilon}{2}\right)^2 + \varepsilon''^2 = \left(\frac{\varepsilon_s - \varepsilon}{2}\right)^2 \quad (7)$$

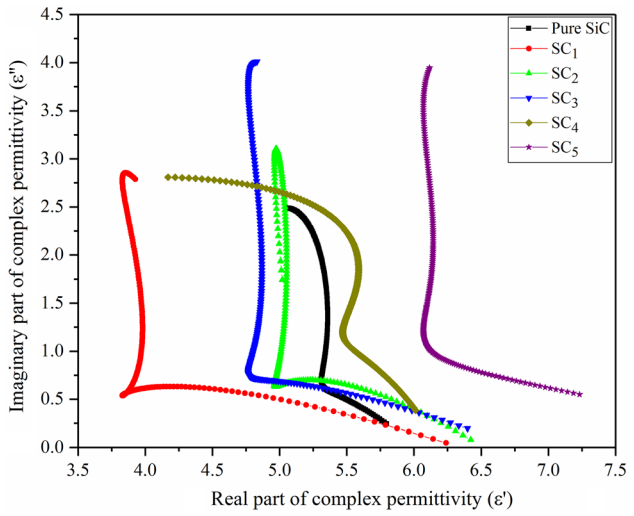

Fig. 11. Cole–Cole curves for the synthesized SWCNT/SiC composites.

where ε_s is the stationary dielectric constant, and ε is the relative dielectric constant at the higher frequency limit. Equation 7 demonstrates that the Cole–Cole curve will be represented in the form of circles; in fact, they are semi-circles. In the Cole–Cole curve, each semi-circle signifies one Debye relaxation process. The more number of semi-circles for a given system represents more number of Debye relaxation processes, signifying enhanced dielectric polarization. The enhanced dielectric relaxation process translates to enhanced microwave absorption performance of the system under consideration. The long tails in the Cole–Cole curves is symbolic of the fact that dominant dielectric loss in such cases is the conduction loss. Therefore, the Cole–Cole curve indicates the degree of polarization relaxation loss and conduction loss involved in a specific system of composite materials. Figure 11 shows the Cole–Cole plots for the synthesized SWCNT/SiC composites. It can be clearly observed from the Cole–Cole plots that the primary absorption mechanism in the pristine SiC system is dielectric relaxation polarization because of the presence of one large and one small semi-circle. However, for the SWCNT/SiC composites, it can be observed that the Cole–Cole plots represent long tails with inconspicuous semi-circles. This is an indication of the fact that in SWCNT dispersed SiC composites, conduction loss is the dominant dielectric loss. With the increase in SWCNT concentration; there would be an enhancement in the conductive loss owing to the conductive nature of CNT. The presence of conductive CNT results in the migration and hopping of electrons in the alternating electromagnetic field culminating into the dissipation of heat energy, paving the path for realizing enhanced microwave absorption. Apart

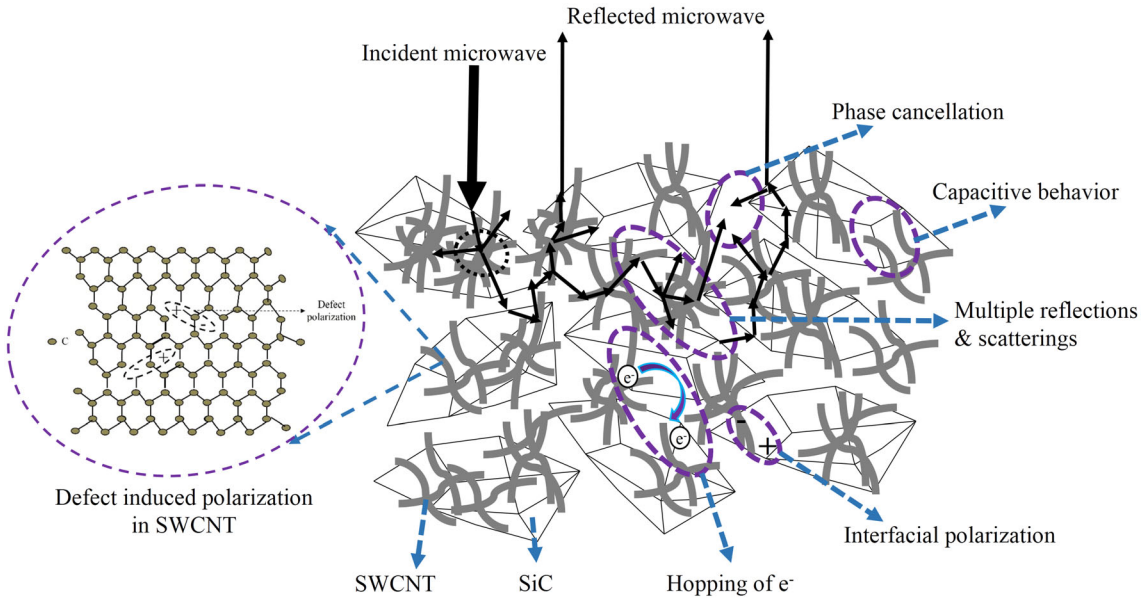

Fig. 12. Representation of various microwave absorbing mechanisms responsible for wave absorption in SWCNT/SiC composites.

from this, due to the increase in SWCNT concentration, a conductive network of CNT is formed, thereby increasing the electrical path length of the incident microwave signals resulting in enhanced absorption. The conductive SWCNT and dielectric SiC particles also form many micro and nano capacitive elements that can store the incident alternating electric field, thus, enhancing the absorption performance of SWCNT/SiC composites. The CNT also serve as sites for multiple scatterings,

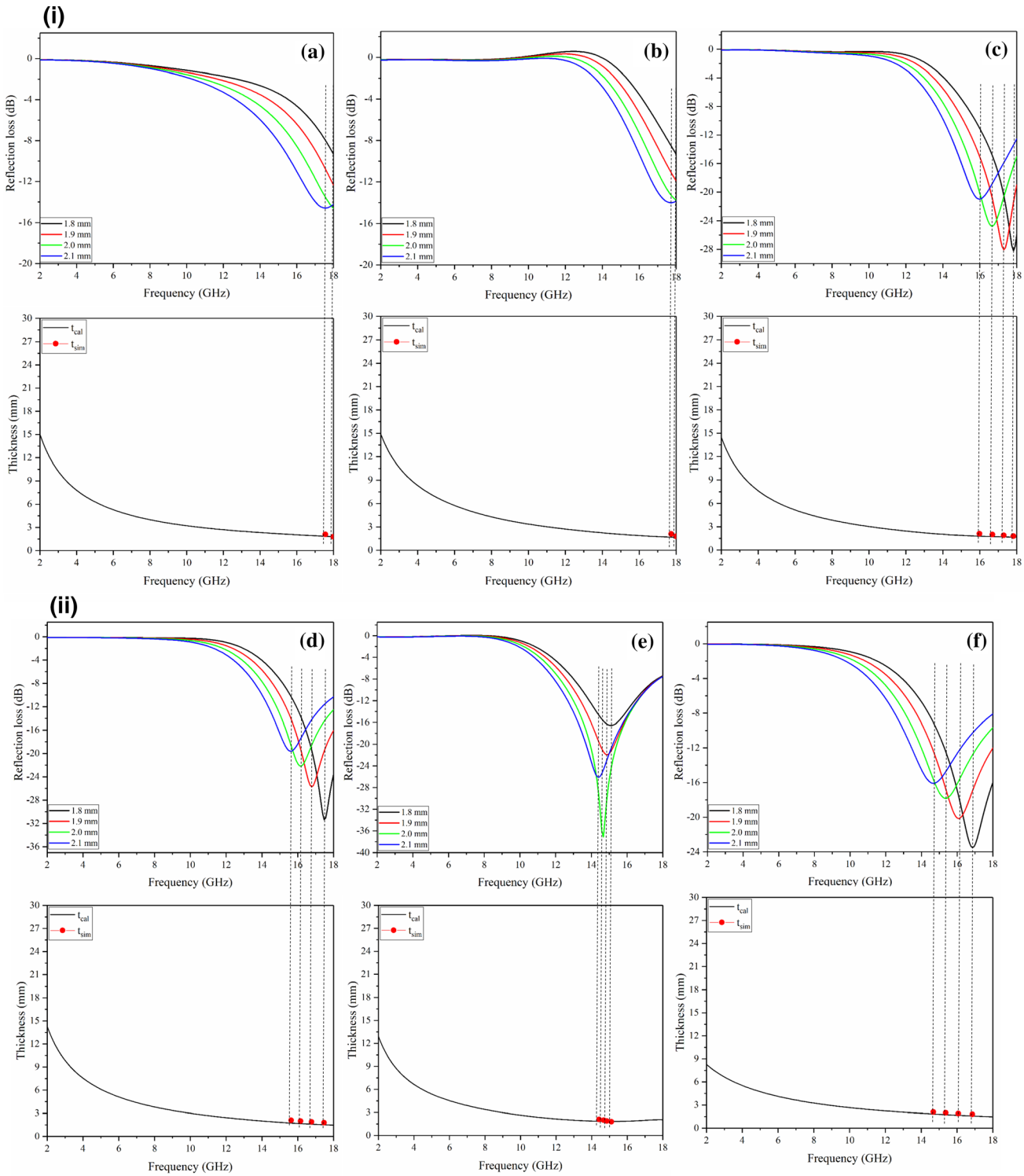

Fig. 13. (i) Dependence of quarter wavelength ($\lambda/4$) effect for the synthesized SWCNT/SiC composites (a) pure SiC, (b) SC_1, and (c) SC_2. (ii) Dependence of quarter wavelength ($\lambda/4$) effect for the synthesized SWCNT/SiC composites (d) SC_3, (e) SC_4, and (f) SC_5.

Table I. Microwave absorption properties of some CNT-based microwave absorbers

Material	Thickness (mm)	Minimum reflection loss (dB)	Bandwidth corresponding to < − 10 dB (GHz)	References
SWCNT/SCPU	2.0	− 22	2–3	33
Fe-filled CNT	1.0	− 31.71	2.9	34
Co-filled MWCNT	3.0	− 39.32	3.47	35
Ni-filled MWCNT	2.0	− 23.1	4.6	36
Fe_3O_4/5wt.% CNT	4.4	− 51.3	3.9	37
CNT@Fe@SiO_2	2.3	− 22.3	3.5	38
H-Fe_3O_4/PPy/CNT	3.0	− 25.9	4.5	39
CNT/Fe_3O_4/rGO/C	1.9	− 54.43	3.2	40
MWCNT	2.5	− 20.5	4.8	41
$NiCo_2$/10wt.% CNT	1.3	− 25.5	4.4	42
SWCNT/Ba-$Fe_{12}O_{19}$	3.0	− 30.79	6.0	43
SiC/2.5wt.% SWCNT	2.0	− 37.11	4.38	This work

reflections, and defect induced dipole polarization, as demonstrated in Fig. 12, which serves as centers for the attenuation of microwave energy. Raman spectra of the composites (Fig. 2) represent a higher I_D/I_G ratio for composite SC_5 as compared to composite SC_1 which signifies that the defect density increases with the rise in SWCNT concentration. These defects result in multiple reflections of the microwave signals, causing the dissipation of microwave energy in the form of heat. The increased concentration of SWCNT also creates an envelope of CNT on the SiC surface. This envelope also aids in the entrapment of microwave signals resulting in the improvement of absorption performance. However, with a much higher concentration of CNT, there would be an extensive network of conductive SWCNT over the dielectric SiC, rendering its high conductive properties. This conductive envelope of CNT reflects the incident microwave signals, thereby deteriorating the attenuation characteristics as in sample SC_5.

The geometrical factor influencing the microwave attenuation characteristics of SWCNT/SiC composites has been investigated using the quarter wavelength theory. This theory signifies the annulment of phases corresponding to the incident and reflected microwave signals due to the destructive interference phenomenon causing the weakening of microwave signals, and comes into play when the geometrical aspect of the absorber, i.e., thickness, satisfies Eq. 8[18]:

$$t_{cal} = [n\,c\,/\,4f\sqrt{(|\varepsilon_r\mu_r|)}] \quad (n = 1, 3, 5, 7, \ldots) \qquad (8)$$

where t_{cal} and n represents the calculated absorber thickness and order of reflection, respectively. The effect of phase cancellation on the developed composites owing to the quarter wavelength effect is depicted in Fig. 13(i) and (ii). It can be realized from Fig. 13 (i)a and b that the contribution of phase annulment in attenuating the microwave signals is not so dominant for pure SiC, and SC_1, as the matching thickness is not in good agreement with the calculated thickness. Conversely, the samples SC_2, SC_3, SC_4, and SC_5, reflect a much better agreement signifying the contribution of the quarter wavelength model in weakening the microwave signals. The synergistic effect of all the aforesaid microwave attenuation mechanisms contributes to improved absorption characteristics for SWCNT/SiC composites.

The microwave absorption properties of some CNT-based microwave absorbers are listed in Table - I and compared with the present work. Table I shows that 2.5 wt.% SWCNT/SiC composite exhibits better reflection loss and absorption bandwidth characteristics with a reasonably thin thickness and less concentration of CNT as compared to the listed composite materials. This indicates that SWCNT/SiC composites may serve as efficient, thin thickness, and low-cost microwave absorber for practical applications.

CONCLUSIONS

A simple mechanical mixing process has been employed to successfully synthesize SWCNT/SiC composites with the help of a ball mill. The

microwave absorption characteristics of SWCNT/SiC composites have shown considerable improvement in the Ku band compared to the pristine SiC counterpart with the addition of a small amount of SWCNT. Strong microwave absorption behavior has been realized for the SWCNT/SiC composite with 2.5 wt.% SWCNT. A minimum RL value of − 37.11 dB at 14.23 GHz and corresponding < − 10 dB absorption bandwidth of 4.38 GHz has been realized for an absorber thickness of 2 mm. In a nutshell, it may be concluded that a slight incorporation of SWCNT can improve the microwave weakening behavior of SWCNT/SiC composites. The onus of improvement in weakening the microwave signals of SWCNT/SiC composites is on various mechanisms, such as conduction loss, defect-induced polarization loss, multiple scatterings, multiple reflections, etc., which work in synergy to consume the microwave energy as heat energy. Therefore, designing SWCNT/SiC composites could prove to be potentially efficient candidates for various applications in the K_u band, such as satellite communications and notch filters.

ACKNOWLEDGMENTS

The author, Samarjit Singh, expresses his earnest gratitude to the Ministry of Human Resources and Development (MHRD), India, for the fellowship. The authors also appreciate various research centers, such as CIR-MNNIT Allahabad, ACMS-IIT Kanpur, and Department of Electronics and Computer Science-IIT Roorkee, for the phase, morphology, and dielectric characterization of the samples.

CONFLICT OF INTEREST

The authors declare that they have no conflict of interest.

REFERENCES

1. S. Singh, S. Shukla, A. Kumar, and D. Singh, *J. Alloys Compd.* 738, 448 (2018).
2. S. Singh and A. Kumar, *Def. Sci. J.* 69, 431 (2019).
3. K. Shi, J. Li, S. He, H. Bai, Y. Hong, Y. Wu, D. Jia, and Z. Zhou, *Curr. Appl. Phys.* 19, 842 (2019).
4. W. Jang, S. Mallesh, S.B. Lee, and K.H. Kim, *Curr. Appl. Phys.* 20, 525 (2020).
5. Z. Shen, J. Chen, B. Li, G. Li, Z. Zhang, and X. Hou, *J. Alloys Compd.* 815, 152388 (2020).
6. S.W. Phang, M. Tadokoro, J. Watanabe, and N. Kuramoto, *Curr. Appl. Phys.* 8, 391 (2008).
7. A. Kumar, V. Agarwala, and D. Singh, *Ceram. Int.* 40, 1797 (2014).
8. R. Panwar and J.R. Lee, *Funct. Compos. Struct.* 1, 032001 (2019).
9. R. Panwar, S. Puthucheri, V. Agarwala, and D. Singh, *J. Electromagn. Waves Appl.* 29, 1238 (2015).
10. J.W. Kim and S.S. Kim, *Mater. Des.* 31, 1547 (2010).
11. S. Puthucheri, I. Singh, M. Najim, R. Panwar, D. Singh, V. Agarwala, and G.D. Varma, *J. Mater. Sci. Mater. Electron.* 27, 7731 (2016).
12. Y. Qing, W. Zhou, S. Huang, Z. Huang, F. Luo, and D. Zhu, *J. Alloys Compd.* 583, 471 (2014).
13. R. Panwar, D.S. Son, and J.R. Lee, *Adv. Compos. Mater* 27, 297 (2018).
14. K. Qian, Z. Yao, H. Lin, J. Zhou, and A.A. Haidry, *Ceram. Int.* 46, 227 (2020).
15. A. Kumar, V. Agarwala, and D. Singh, *Prog. Electromagn. Res. M.* 29, 223 (2013).
16. Z. Wang, P. Zhao, D. He, Y. Cheng, L. Liao, S. Li, Y. Luo, Z. Peng, and P. Li, *Phys. Chem. Chem. Phys.* 20, 14155 (2018).
17. H. Xu, S. Bie, Y. Xu, W. Yuan, Q. Chen, and J. Jiang, *Compos. Part A: Appl. Sci. Manuf.* 80, 111 (2016).
18. S. Singh, A. Kumar, S. Agarwal, and D. Singh, *J. Magn. Magn. Mater.* 503, 166616 (2020).
19. J. Kuang, P. Jiang, F. Ran, and W. Cao, *J. Alloys Compd.* 687, 227 (2016).
20. A. Kumar, V. Agarwala, and D. Singh, *Adv. Powder Technol.* 25, 483 (2014).
21. P. Chen, S. Jing, Y. Chu, and P. Rao, *J. Alloys Compd.* 730, 42 (2018).
22. Y. Zhang, Y. Liu, X. Wang, Y. Yuan, W. Lai, Z. Wang, X. Zhang, and X. Liu, *J. Mater. Chem. C.* 5, 11847 (2017).
23. S. Singh, A. Sinha, R.H. Zunke, A. Kumar, and D. Singh, *Adv. Powder Technol.* 29, 2019 (2018).
24. P. Wang, L. Cheng, Y. Zhang, and L. Zhang, *ACS Appl. Mater. Interfaces* 9, 28844 (2017).
25. A. Kumar, S. Singh, and D. Singh, *J. Alloys Compd.* 772, 1017 (2019).
26. K. Yan, F. Yin, C. Pang, X. Zuo, Q. Zhang, L. Shen, R. Fan, and N. Bao, *RSC Adv.* 9, 41817 (2019).
27. D. Jiao, X. Fan, N. Tian, C. You, and G. Zhang, *J. Alloys Compd.* 703, 13 (2017).
28. A. Kumar, V. Agarwala, and D. Singh, *Adv. Mater. Res.* 585, 62 (2012).
29. Saurabh, A.K. Maurya, S. Singh, and A. Kumar, *Def. Sci. J.* 69, 437 (2019).
30. B. Zhao, X. Guo, W. Zhao, J. Deng, G. Shao, B. Fan, Z. Bai, and R. Zhang, *ACS Appl. Mater. Interfaces* 8, 28917 (2016).
31. P.J. Bora, I. Azeem, K.J. Vinoy, P.C. Ramamurthy, and G. Madras, *ACS Omega* 3, 16542 (2018).
32. S. Singh, A. Kumar, and D. Singh, *J. Alloys Compd.* 823, 153780 (2020).
33. Z. Liu, G. Bai, Y. Huang, F. Li, Y. Ma, T. Guo, X. He, X. Lin, H. Gao, and Y. Chen, *J. Phys. Chem. C* 111, 13696 (2007).
34. D.L. Zhao, X. Li, and Z.M. Shen, *J. Alloys Compd.* 471, 457 (2009).
35. Z. Zheng, B. Xu, L. Huang, L. He, and X. Ni, *Solid State Sci.* 10, 316 (2008).
36. T. Zou, H. Li, N. Zhao, and C. Shi, *J. Alloys Compd.* 496, L22 (2010).
37. L. Zhu, X. Zheng, M. Chen, and R. Yu, *RSC Adv.* 7, 26801 (2017).
38. H. Lv, G. Ji, H. Zhang, and Y. Du, *RSC Adv.* 5, 76836 (2015).
39. R.B. Yang, P.M. Reddy, C.J. Chang, P.A. Chen, J.K. Chen, and C.C. Chang, *Chem. Eng. J.* 285, 497 (2016).
40. K. Zhang, Q. Zhang, X. Gao, X. Chen, Y. Wang, W. Li, and J. Wu, *J. Alloys Compd.* 748, 706 (2018).
41. S. Yun, A. Kirakosyan, S. Surabhi, J.R. Jeong, and J. Choi, *J. Mater. Chem. C.* 5, 8436 (2017).
42. B. Wang, C. Zhang, C. Mu, R. Yang, J. Xiang, J. Song, F. Wen, and Z. Liu, *J. Magn. Magn. Mater.* 471, 185 (2019).
43. K. He, L. Yu, L. Sheng, K. An, Y. Ando, and X. Zhao, *Jpn. J. Appl. Phys.* 49, 125101 (2010).